Journal of Power Sources 256 (2014) 250–257

Contents lists available at ScienceDirect

Journal of Power Sources

journal homepage: www.elsevier.com/locate/jpowsour

Performance comparison between high temperature and traditional proton exchange membrane fuel cell stacks using electrochemical impedance spectroscopy

Ying Zhu, Wenhua H. Zhu, Bruce J. Tatarchuk*

Center for Microfibrous Materials, Department of Chemical Engineering, 212 Ross Hall, Auburn University, Auburn, AL 36849-5127, USA

HIGHLIGHTS

- A commercial HT-PEM fuel cell stack is operated at 160 °C with pure H_2 supplement.
- A non-ideal EC model is proposed to simulate both types of PEM fuel cell stacks.
- Fuel cell processes are mechanistically discriminated by EC simulation.
- Stack performance is compared between HT and traditional PEM fuel cell stacks.
- HT-PEM fuel cell stack has less polarization loss and better water management.

ARTICLE INFO

Article history:
Received 29 October 2013
Received in revised form
5 January 2014
Accepted 10 January 2014
Available online 18 January 2014

Keywords:
High temperature PEM fuel cells
PEM fuel cells
Impedance spectroscopy
Equivalent circuit simulation

ABSTRACT

A temperature above 100 °C is always desired for proton exchange membrane (PEM) fuel cell operation. It not only improves kinetic and mass transport processes, but also facilitates thermal and water management in fuel cell systems. Increased carbon monoxide (CO) tolerance at higher operating temperature also simplifies the pretreatment of fuel supplement. The novel phosphoric acid (PA) doped polybenzimidazole (PBI) membranes achieve PEM fuel cell operations above 100 °C. The performance of a commercial high temperature (HT) PEM fuel cell stack module is studied by measuring its impedance under various current loads when the operating temperature is set at 160 °C. The contributions of kinetic and mass transport processes to stack impedance are analyzed qualitatively and quantitatively by equivalent circuit (EC) simulation. The performance of a traditional PEM fuel cell stack module operated is also studied by impedance measurement and EC simulation. The operating temperature is self-stabilized between 40 °C and 65 °C. An enhancement of the HT-PEM fuel cell stack in polarization impedance is evaluated by comparing to the traditional PEM fuel cell stack. The impedance study on two commercial fuel cell stacks reveals the real situation of current fuel cell development.

1. Introduction

The application of proton exchange membrane (PEM) fuel cell systems keeps improving in pursuit of higher performance but lower cost. A higher operating temperature provides faster kinetics and better thermal management. It increases not only the energy efficiency but also the economical efficiency of cell systems. The most stressed benefit of high temperature operation is the more competitive hydrogen (H) adsorption onto electrode catalyst. The CO tolerance of carbon-supported platinum (Pt) significantly increases up to 30,000 ppm when PEM fuel cells are operated at about 200 °C [1]. However, an elevated operating temperature greatly challenges the properties of cell components and the portability of cell applications. The inevitable dehydration of a traditional perfluorosulfonic acid (PFSA) membrane breaks down its mechanical support and decreases its proton conductivity. The choice of an optimum operation temperature is the trade-off between kinetics, heat utilization, material availability, operation feasibility, and other performance and economy related factors.

Phosphoric acid (H_3PO_4, abbreviate to PA) doped polybenzimidazole (PBI) membrane is proved to be one of the most promising alternatives to the traditional PFSA membrane for high temperature (HT) operations [2]. The advantages of PBI polymers include high glass transition temperature [3], low cost [4], great thermal stability [4], and excellent textile fiber properties [5]. With these features, PBI polymers are competent to be the excellent

* Corresponding author. Tel.: +1 (334) 844 2023; fax: +1 (334) 844 2063.
E-mail address: tatarbj@auburn.edu (B.J. Tatarchuk).

0378-7753/$ – see front matter © 2014 Elsevier B.V. All rights reserved.
http://dx.doi.org/10.1016/j.jpowsour.2014.01.049

choice for membrane backbones. After doping with PA units, the interactions between acid units and PBI backbones provide additional charge carriers for proton conduction [6]. Based on almost twenty years of research on high temperature membranes, the operation of PEM fuel cells at temperature over 100 °C has been accomplished; however, the commercialization of its application is still in the starting stage.

Electrochemical impedance spectroscopy (EIS) is one of the most powerful techniques to non-destructively assess the *in-situ* dynamic responses of fuel cell systems. The impedance data measured by EIS can be analyzed and interpreted by equivalent circuit (EC) simulation. An EC model is a physical circuit consisting of electrical elements. It produces similar load responses to the cell systems under test. Cell impedance is a combination of cell losses contributed by different chemical and physical processes in cell systems. EC model can be used to dissect the cell impedance and ascribe each part to certain cell processes. In this way, it is able to quantitatively and qualitatively study which and to what degree kinetics and mass transfer processes limit cell outputs [7].

The impedance work related to HT-PEM fuel cells began with the conductivity measurement of PBI-based films at the end of 1990s [8,9]. The EIS was utilized only as an auxiliary method in these work. The application of EIS to an HT membrane electrode assembly (MEA) [10] or a fully constructed HT-PEM fuel cell [11] was rarely found until 2005, focusing on the effects of relative humidity (RH). The impedance study of a single cell assembly, named Celtec®-P series 1000 MEA (BASF Fuel Cell), was published in 2006 [12]. This work provided a well developed case of EIS application to the PA-PBI based HT-PEM fuel cell, but without EC simulation. At the same time, Jingwei Hu and his co-workers [13–15] published a series of impedance studies of their self-made PA-PBI HT-MEAs operated at 150 °C and constant load. EC simulation and degradation tests were also included in their work. Later, more attentions were paid to the EIS applications to PA-PBI based HT-PEM fuel cells. However, with less than ten-year development, no general consensus has been achieved neither on EC models nor impedance interpretations.

This work highlights the advantages of EIS technique and EC simulation in their application to dynamic characterization and evaluation of electrochemical energy systems. The purpose of this work is to compare the performance of the HT-PEM fuel cell stack to the traditional one by impedance measurement and EC simulation. The advantages of the HT-PEM fuel cell stack over the traditional one is revealed by the significantly improved polarization losses. The results of impedance spectra and EC simulation in this work also provide experimental data of HT-PEM fuel cell systems for further mechanism validation and stack diagnostics.

2. Experimental descriptions

2.1. HT-PEM fuel cell stack

The commercial HT-PEM fuel cell stack module (Serenus 166Air C Fuel Cell Evaluation Kit, Serenergy Inc.) under research is featured by PA-PBI membranes. The active area of the membrane electrode assembly (MEA) is about 45 cm^2. The whole stack consists of 65 planar single cells, that is 66 electrode plates. The nominal power at its beginning of life (BOL) is about 1 kW. The stack is capable to be operated in the temperature range between 100 °C and 175 °C, with an optimum at 160 °C. It can be fueled not only with pure hydrogen (H_2) but reformate gases.

Pure H_2 was supplied to the anode during impedance measurement. Ambient air was supplied through a blower to the cathode. A purge valve (Bürkert 6011, 2/2-way Miniature Solenoid Valve) was installed at the fuel outlet to provide a dead-end anode configuration. The pressure of the stack system was stable at 45 mbar (0.6527 psig) by a proportional valve (Bürkert 2835, 2/2-way proportional valve) installed at the H_2 inlet. The valve was controlled by a digital controller (Bürkert 8611, eControl) and a pressure sensor (Bürkert 8314, pressure transmitter) by feedback mechanism. An illustration of the experimental configuration is shown in Fig. 1. The bold black solid lines indicate the electric circuit connections. And the thin black solid lines refers to signal channels for data communication.

EIS measurement was conducted by Gamry FC350™ fuel cell monitor (Gamry Instruments), in conjunction with TDI-Dynaload® RBL488 programmable load. A LabVIEW (National Instruments) based program, called Embedded Fuel Cell Control Unit (EFCU) (Serenergy Inc.) was installed to monitor the module status during

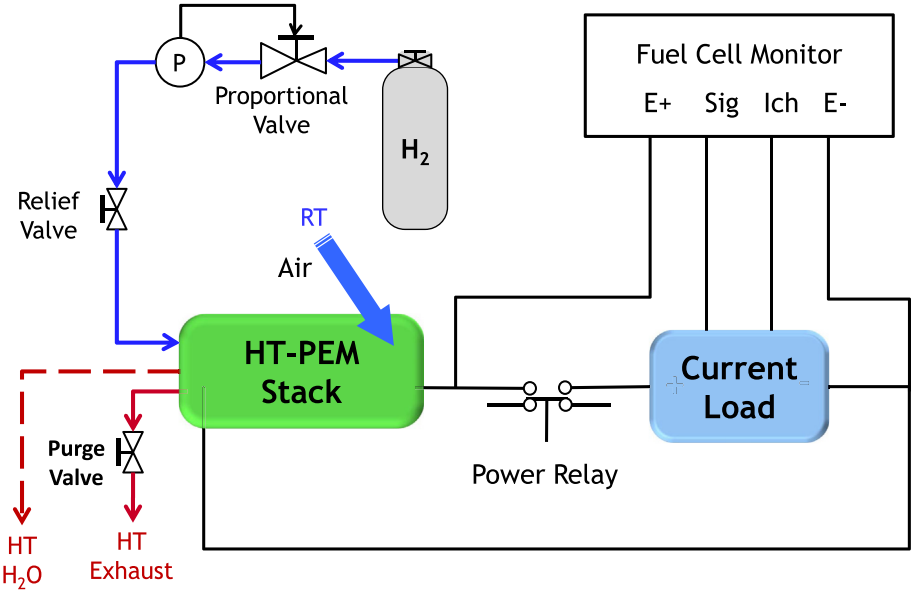

Fig. 1. Illustration of the electrical configuration for obtaining impedance data from the HT-PEM fuel cell stack. A fuel cell monitor (Gamry Instruments) and a current load (TDI-Dynaload) are connected to this measuring circuit. Solid arrows refer to gas inlet and outlet of the anode. Dashed arrow refers to water outlet of the cathode. Bold lines refer to electrical connections, and thin lines refer to signal channels.

its operation. A set of impedance data of the whole stack module (including the blower, heater, bleeder resistors, sensors, and other electronic devices embedded in the system) was measured during cell operation. The operating temperature was set at 160 °C. The stack was preheated to the set temperature and self-stabilized around this operating temperature. The impedance measurement was conducted after the stack reaching a stable condition. A *dc* current of 4.5 A, 9 A, 12 A, 13.5 A, and 15 A, corresponding to the current density of 100 mA cm^{-2}, 200 mA cm^{-2}, 267 mA cm^{-2}, 300 mA cm^{-2}, and 333 mA cm^{-2}, was loaded to the stack from low to high. The frequency swept from 10 kHz to 0.1 Hz at a rate of 10 points per decade under each current load setting.

2.2. Traditional PEM fuel cell stack

The traditional PEM fuel cell stack module, named Nexa™ fuel cell system (Ballard Power Systems Inc.), was studied by EIS measurement. Nexa system is a 47-cell stack module with an unregulated *dc* power of 1.2 kW. Its output current can reach 44 A. The stack voltage normally rises up to 41 V at open circuit and 26 V at full load. The fuel cell geometric working area is estimated as *ca.* 122 cm^2 due to the inexistence of manufacturing data [16,17]. The automated operation is maintained by an embedded controller board. H_2 was supplied to the stack anode at 5.0 psig, and air was supplied through a blower to the stack cathode at 2.2 psig.

An experimental configuration similar to the one used for HT-PEM fuel cell stack (Fig. 1) was employed to obtain the impedance data of the Nexa stack, which include the impedance contributed by the blower, the heater, and the embedded controller board. Gamry FC350™ fuel cell monitor in conjunction with TDI-Dynaload® RBL488 programmable load was utilized to measure the stack impedance under *dc* current loads of 12.2 A, 24.4 A, and 32.5 A from low to high. The corresponding current densities were 100 mA cm^{-2}, 200 mA cm^{-2}, and 267 mA cm^{-2}, consistent with the load condition of the HT-PEM system. The measuring frequency swept from 10 kHz to 0.01 Hz. The operating temperature of the Nexa stack module was automatically stabilized between 40 °C and 65 °C.

3. Results and discussion

3.1. Impedance spectra of HT-PEM fuel cell stack

Five impedance spectra of the HT-PEM fuel cell stack module measured under different current loads are plotted together in one Nyquist plot (Fig. 2). The operating temperature is set at 160 °C. When the load current increases from 100 mA cm^{-2} to 333 mA cm^{-2}, a decrease of total stack impedance is observed. It is mainly contributed by the decrease of the impedance arcs dominating the frequency range lower than 100 Hz. The smaller intercept of the spectra and the real axis (the one closer to the origin of Nyquist plot, measured at the frequency point higher than 1000 Hz) almost keeps constant at around 15 Ω cm^2 despite the change of the stack load. But the larger intercept of the spectra and the real axis (the one further from the origin of Nyquist plot, measured at the frequency point lower than 1 Hz) decreases significantly from approximately 70 Ω cm^2 to 40 Ω cm^2 with increasing current density. No significant change of the impedance arc dominating high frequency range can be observed from Fig. 2. High frequency inductive impedance also keeps at a steady status with the change of the stack load.

3.2. EC simulation of HT-PEM fuel cell stack

3.2.1. EC model for simulation

A fully constructed HT-PEM fuel cell and stack based on PA-PBI membranes is quite a new technology, not to mention a well established HT-PEM fuel cell stack. The published impedance work on this type of fuel cells is still limited. However, there is no agreement between the results of those work. Different EC models are proposed by different research groups to interpret their impedance data. The ohmic resistance and wiring induction are involved in all published impedance measurement. Up to three arcs are reported for the contributions to the total polarization impedance [12,18–20], corresponding to a three time constant EC model. But a two time constant EC model is preferred by some research groups [21,22]. The difference lies in their different consideration of the low frequency impedance arc, which cannot be well separated from the middle frequency arc under some measuring conditions.

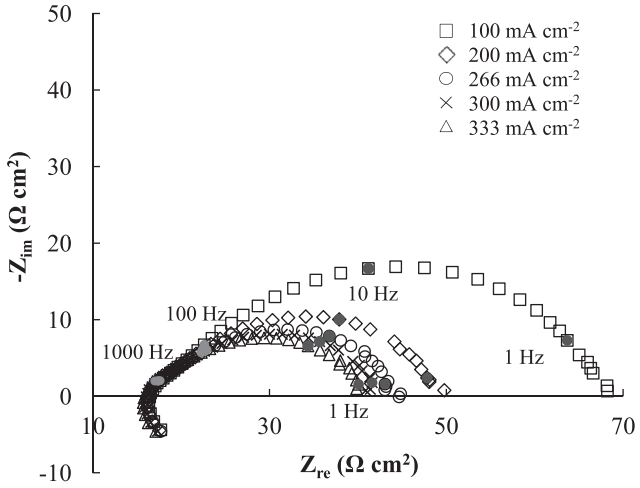

Fig. 2. Five impedance spectra of the HT-PEM fuel cell stack measured under *dc* current density of (□) 100 mA cm^{-2}, (◇) 200 mA cm^{-2}, (○) 267 mA cm^{-2}, (×) 300 mA cm^{-2}, and (△) 333 mA cm^{-2}. The impedance data measured at frequency of 1000 Hz, 100 Hz, 10 Hz, and 1 Hz of each spectra are marked with solid dots. The operating temperature is set at 160 °C. Pure H_2 is supplied to the stack anode at around 45 mbar and ambient temperature. Ambient air is taken into the stack cathode by the blower.

In this work, a three time constant non-ideal EC model (Fig. 3) is proposed to simulate the HT-PEM fuel cell stack. It consists of one pure resistor R_Ω, one paralleled (C_aR_a) sub-circuit, one paralleled (Q_cR_c) sub-circuit, one finite diffusion element (FDE) *O*, and one wiring inductor *L*. In this EC model, one constant phase element (CPE) Q_c is used to replace the ideal capacitor and reflect the non-ideality of the processes on cathode electrode caused by the inhomogeneous characterization of the electrode surface. The detail explanations are presented in the following section of EC interpretation.

The impedance spectrum measured at a *dc* current load of 9 A (200 mA cm^{-2}) is simulated by the non-ideal EC model (Fig. 3). The measured data and its fitting curve are shown in Fig. 4. The smaller intercept on the real axis refers to the ohmic resistance (R_Ω) of the stack module. The difference between two intercepts on the real axis refers to the polarization resistance (R_p) of the stack, which is a combined contribution of activation and concentration processes. The small capacitive arc dominating the high frequency region is simulated by the paralleled (C_aR_a) sub-circuit. This arc has a summit

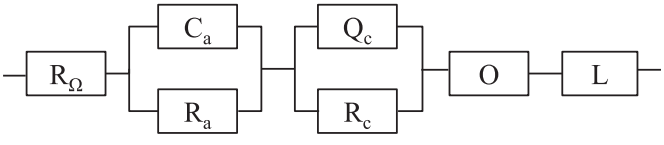

Fig. 3. The non-ideal EC model proposed to simulate the HT-PEM fuel cell stack.

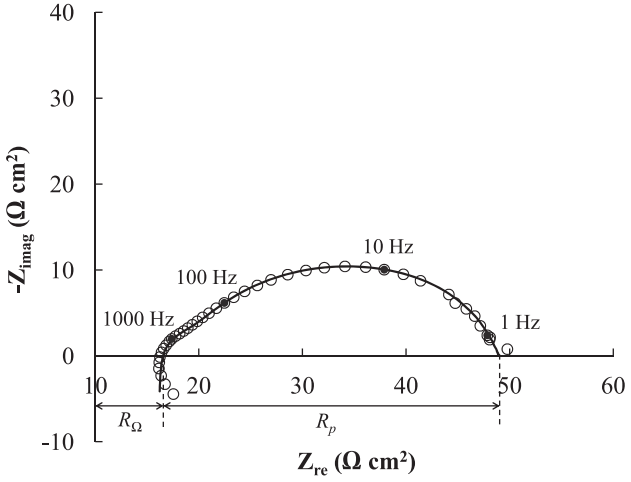

Fig. 4. The impedance spectrum of the HT-PEM fuel cell stack measured under a current load of 9 A (200 mA cm^{-2}). The impedance data measured at frequency of 1000 Hz, 100 Hz, 10 Hz, and 1 Hz are marked with solid dots (•). The operating temperature is set at 160 °C. The fitting curve is simulated by the non-ideal EC model (Fig. 3). Pure H_2 is supplied to the stack anode at around 45 mbar and ambient temperature. Ambient air was taken into the stack cathode by the blower.

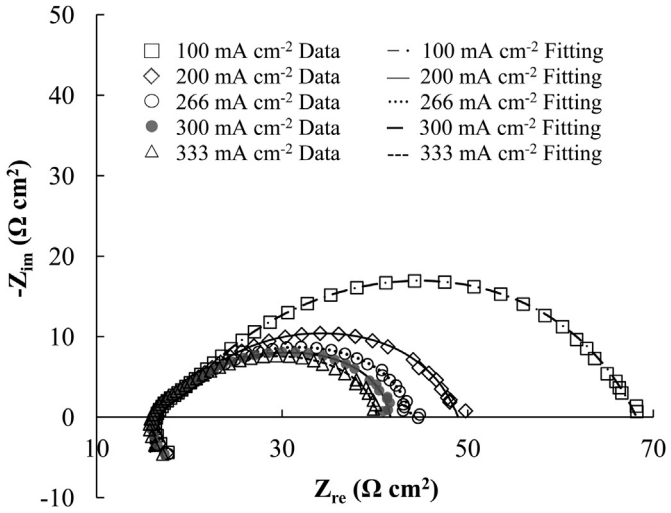

Fig. 5. The impedance spectra of the HT-PEM fuel cell stack measured under various current loads. The operating temperature is set at 160 °C. The fitting curves are simulated by the non-ideal EC model (Fig. 3). Pure H_2 is supplied to the stack anode at around 45 mbar and ambient temperature. Ambient air is taken into the stack cathode by the blower.

frequency at about 680 Hz. The depressed large capacitive impedance arc spanning over the rest frequency region is simulated as two overlapped capacitive arcs. The middle frequency arc, which has a summit frequency at around 20 Hz, is simulated by the paralleled (Q_cR_c) sub-circuit. This impedance arc is much larger than others and dominates the stack impedance. The low frequency arc is simulated by the diffusion element and gives very limited contribution to the stack impedance under this operating condition.

The non-uniqueness of EC model challenges its application to impedance interpretation. It can be overcome by validating the EC model under different cell configurations and operating conditions. The more impedance spectra measured from the testing system and other similar systems, the more valid is the EC model. In this work, the proposed non-ideal EC model is applied to the impedance spectra measured under varying loads (Fig. 5). The simulation curves show great goodness of fit with the changing current density. The fitting values of each EC elements and their changes with current loads are analyzed below to perform EC element interpretation. The impedance spectra and EC simulations published in other research work are considered as references to support our results.

3.2.2. EC element interpretation

3.2.2.1. Ohmic resistance. The ohmic loss refers to pure resistive losses and can be simulated by one ideal resistor R_Ω. It consists of resistances contributed by membranes, electrodes, catalyst layers, gas diffusion layers, component connections, and any other hardware connected to the measuring system, such as wires, heaters, blowers, and controller boards. However, it is difficult to discriminate their impedance one from another. The variation of ohmic loss with changing current load reflects the change of proton conductivity of the membranes.

3.2.2.1.1. Proton conductivity mechanism. The mechanism of proton conductivity changes with PA doping level. Generally, PA is doped onto the PBI backbone in two different manners. As far as the doping level is lower than two molecules of PA per repeat unit of PBI [23], the acids are stably linked to the PBI structure by H bonding. The conductivity at low PA doping level comes from a cooperative movement of two protons along the polymer-PA anion chain [9], that is one proton hopping away from an acid anion to form a N–H bond with the polymer and this anion accepting the proton hopping from another N–H bond at the same time. This type of proton migration provides great contribution to membrane conductivity but is not enough for fuel cell applications. Experimental data [24] support that the conductivity of PA doped PBI significantly increases with an increasing doping level of PA when more than two molecules of PA per repeat unit of PBI are doped. Other than the PA molecular bounded to PBI by H bonding, the rest of doped PA molecular form $H_2PO_4^-$ by self-ionization and self-dehydration [6]:

$$5H_3PO_4 \rightleftharpoons 2H_4PO_4^+ + H_3O^+ + H_2PO_4^- + H_2P_2O_7^{2-} \quad (1)$$

The proton conduction is described as a proton hopping mechanism along the anionic chains of $H_2PO_4^-/HPO_4^{2-}$ [6]. This mechanism provides the main attribution to proton conductivity and significantly increases the conductivity of PA-PBI membranes to meet the requirement of EC application.

In PA-PBI system, water is no longer the essential contributor to proton conductivity. This feature enables fuel cell operations above 100 °C. However, the presence of water still has non-negligible effects on proton conductivity of PA-PBI membranes. Additional proton carriers can be formed by dissociating acid molecular in water [6] and increase the proton conductivity.

$$H_3PO_4 + H_2O \rightleftharpoons H_3O^+ + H_2PO_4^- \quad (2)$$

The situation changes when the content of water continuously increases. The reducing concentration of charge carriers due to excessive water content leads to a decrease of conductivity.

3.2.2.1.2. Dependence on current density. Our experimental data (Fig. 5) and simulation results (Fig. 6) present a relevant stable value of ohmic resistance (R_Ω) when the current density is lower than 267 mA cm^{-2}. However, it slightly decreases when the current density increases from 267 mA cm^{-2} to 333 mA cm^{-2}. A decrease of ohmic resistance with increasing current density was reported [20,22,25], but Zhang [18] also reported a stable ohmic resistance with the change of current load when the current density went

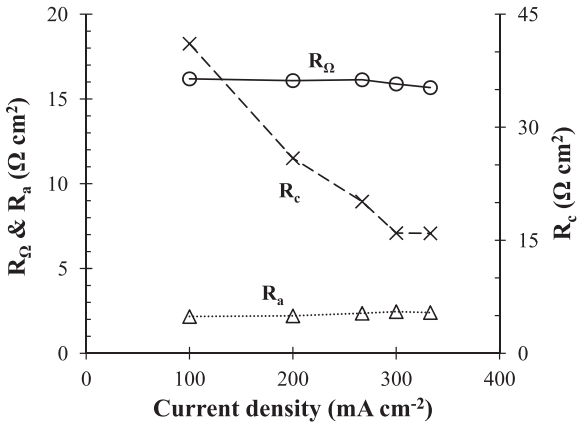

Fig. 6. The dependence of stack ohmic resistance (R_Ω), anode activation resistance of HOR process (R_a), and cathode activation resistance of ORR process (R_c) on current density. R_Ω and R_a are plotted with the primary vertical axis at left, and R_c is plotted with the secondary vertical axis at right. The values are simulated from the non-ideal EC model (Fig. 3).

larger than 1.0 A cm^{-2}. The conductivity following the hopping mechanism changes with temperature and membrane water content. It is theoretically independent on current load. The stable value of R_Ω at low current densities represents a stable conduction process throughout the current density range below 267 mA cm^{-2}. More water is produced under higher current loads. When the current density increases to over 267 mA cm^{-2}, water content of MEAs slightly increases due to the disequilibrium between produced water and purged water. Thus, the slight decrease of R_Ω at higher current loads is observed because the small amount of water increases the proton conductivity.

3.2.2.2. Hydrogen oxidation reaction (HOR). The electrode process occurring on the anode of a hydrogen–oxygen (H_2–O_2) fuel cell is hydrogen oxidation reaction (HOR). It has been widely accepted that the rate determining step (RDS) of HOR is the transfer process of electrons from the absorbed hydrogen atoms to the electrode [26]:

$$M\cdots H \rightleftharpoons \left(M + e^-\right) + H^+ \tag{3}$$

HOR kinetics is much faster than oxygen reduction reaction (ORR) kinetics and other cell processes. When the frequency sweeps from high to low values, the impedance arc of HOR charge transfer process appears right after the wiring inductive loop. It usually behaves as a semi-circle much smaller than other impedance arcs. A dominating frequency range from about 100 Hz up to 1000 Hz or even higher [12,18–22,25,27] was reported for this process. Following this theory, the (C_aR_a) sub-circuit in the proposed EC model (Fig. 3) is employed to simulate the charge transfer process occurring over anode/electrolyte interfaces. R_a refers to the resistance of electron transfer processes (Eq. (3)) occurring on anode electrodes. C_a refers to the double-layer capacitance caused by the charge accumulation and separation in anode/electrolyte interfaces. The kinetics of HOR process is so fast that no significant effect of current density is expected on HOR, especially when the cell is operated under low current densities. As shown in Fig. 6, the charge transfer resistance of HOR (R_a) keeps at a stable value with the change of current load.

3.2.2.3. Oxygen reduction reaction (ORR). The electrode process occurring on the cathode of H_2–O_2 fuel cells is ORR. Its kinetics is very sluggish comparing to HOR process. The impedance of ORR process usually dominates the performance of total cell systems. No consensus has been reached after decades of ORR mechanism study. The main controversy lies between whether the charge transfer process of ORR is the RDS [28] or the adsorption process of oxygen molecular on catalyst surface is the RDS [29]. The generally accepted mechanism for PEM fuel cell systems considers the charge transfer process as the RDS of ORR process but with a change of Tafel slope at higher overpotential [28].

The large capacitive impedance arc spanning over hundreds of hertz down to several hertz (Fig. 2) is ascribed to the activation process of ORR. Its behavior and dominating frequency range obtained in this work keep consistency with the results of other published cases of HT-PEM impedance study [12,18–20,27]. In this work, the sub-circuit (Q_cR_c) in the proposed EC model (Fig. 3) is used to simulate the activation process of ORR. The ORR activation resistance R_c drops about 25 Ω cm^2 when the current density increases from 100 mA cm^{-2} to 300 mA cm^{-2} (Fig. 6). The acceleration of electrons at higher current density enhances the charge transfer process and lowers the impedance of ORR process. However, the dependence of R_c on current density changes when the current density increases to more than 300 mA cm^{-2}. It keeps at a stable value when the current density increases from 300 mA cm^{-2} to 333 mA cm^{-2} (Fig. 6). The RDS of ORR process changes in this current density range when the adsorption of oxygen molecular on catalyst surface gradually lags behind the charge transfer process. This explanation could be further validated by continuously measuring cell impedance at even higher current densities.

3.2.2.4. Finite diffusion process. The impedance arc dominating the frequency lower than 1 Hz mostly merges with the ORR activation impedance arc. Only a small tail following the ORR impedance arc can be observed from the Nyquist plot (Fig. 2). The low frequency impedance arc is contributed by the diffusion process of O_2 to the cathode electrode. The finite diffusion element (FDE) *O* is employed in the non-ideal EC model to simulate the low frequency diffusion process. The two simulation parameters of FDE are *B* and $Y_{O,0}$. *B* is the time constant parameter in the unit of sec$^{1/2}$. It reflects the rate of diffusion process. $Y_{O,0}$ is the admittance parameter in the unit of S sec$^{1/2}$, that is the reciprocal of Ω sec$^{-1/2}$. Its magnitude is defined based on the model of Warburg element, as [30]:

$$Y_{O,0} = \frac{n^2F^2A}{RT}\left(\frac{1}{D_O^{1/2}C_O^*} + \frac{1}{D_R^{1/2}C_R^*}\right)^{-1} \tag{4}$$

where, n is the stoichiometric number of electrons involved in the reduction reaction; F is the Faraday constant; R is the ideal gas constant; D_O and D_R are diffusivity of oxidized species and reduced species, respectively; and C_O^* and C_R^* are their bulk concentrations, respectively. R_O is the impedance of FDE [7]calculated at $\omega = 0$, equivalent to the value of R in a paralleled (CR) circuit:

$$R_O = Z_{O,(\omega=0)} = \lim_{\omega\to 0}\frac{\tanh\left(B\sqrt{j\omega}\right)}{Y_{O,0}\sqrt{j\omega}} = \lim_{\omega\to 0}\frac{B\sqrt{j\omega}}{Y_{O,0}\sqrt{j\omega}} = \frac{B}{Y_{O,0}} \tag{5}$$

R_O decreases when the current density increases from 100 mA cm^{-2} to 200 mA cm^{-2} (Fig. 7). A reversed trend is then observed with further increase of current density. Ambient air is fed to the cathode as the source of O_2. As the ORR process is enhanced at higher current density, the concentration of O_2 decreases and fails to keep at the constant level due to a faster consumption by the ORR process. The diffusion process of O_2 to the cathode lags behind

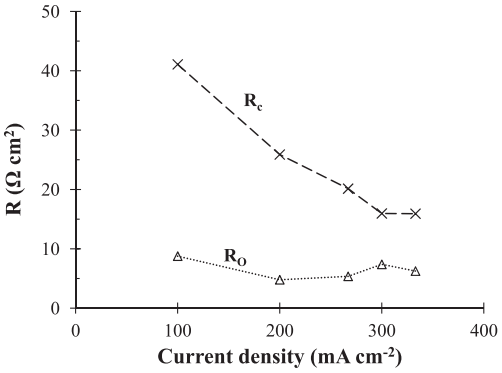

Fig. 7. Comparison between the resistance of ORR process R_c and the equivalent diffusion resistance R_O calculated from Eq. (5). The values are simulated from the impedance spectra of HT-PEM fuel cell stack at an operating temperature of 160 °C and changing current density.

the electrode reaction at higher current density and gives large impedance to the stack performance. When the current density increases to over 300 mA cm^{-2}, the RDS of ORR process changes to the adsorption process of oxygen molecular. It relieves the lag of O_2 diffusion to the electrode, and slightly decreases the diffusion resistance. The explanation can be further validated by operating the HT-PEM fuel cell stack by varying the concentration of O_2 in the cathode supplement and changing the ratio of H_2 and O_2. Comparing to the values of ORR resistance (Fig. 7), the diffusion process does not give much contribution to the impedance of HT-PEM fuel cell stack under the operating condition during impedance measurement.

3.3. EC simulation of traditional PEM

One widely accepted interpretation of PEM fuel cell impedance is to separate the polarization impedance according to anodic and cathodic processes. The time constants of HOR and ORR processes, the main impedance contributions of anodic and cathodic electrodes, are quite different that their impedance arcs can be clearly distinguished from each other. Following this idea, an ideal EC model (Fig. 8) consisting with one ohmic resistor, three (*CR*) sub-circuits, and one wiring inductor was used to simulate the Nexa™ PEM fuel cell stacks in our previous work [17]. Three parallel (*CR*) sub-circuits were ascribed to anode HOR process (C_aR_a), cathode ORR process (C_cR_c), and cathode finite diffusion process ($C_{diff}R_{diff}$), respectively in sequence from high frequency to low frequency. The EC model with only ideal circuit elements was used to facilitate PSpice simulation.

The newly proposed non-ideal EC model (Fig. 3) shows great fitness to the impedance spectra measured from the HT-PEM fuel cell stack. It inspires the idea that the non-ideal EC model can be used to simulate the traditional PEM fuel cell stack. As expected, its simulation result shows great consistency to the impedance spectra measured at 200 mA cm^{-2} (Fig. 9). The small impedance arc simulated by the parallel (C_aR_a) appears in the frequency range larger than 100 Hz. It refers to the activation process of HOR on

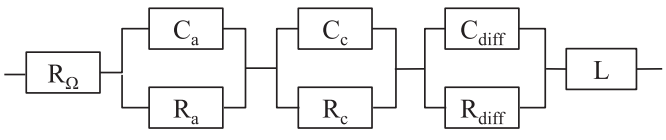

Fig. 8. The ideal EC model with three time constants.

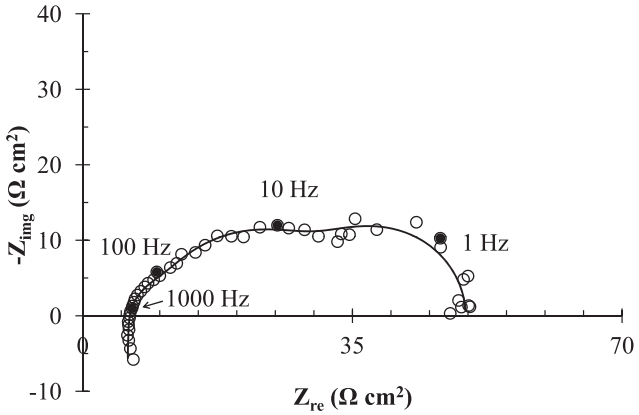

Fig. 9. The impedance spectrum of the traditional PEM fuel cell stack (○) measured under a *dc* current load of 24.4 A (200 mA cm^{-2}). The solid fitting curve is simulated from the non-ideal EC model (Fig. 3). Pure H_2 and ambient air are supplied to the stack.

anode electrodes. The large impedance arcs spanning over from several Hertz up to 100 Hz is contributed by the activation process of ORR on cathode electrodes. For the HT-PEM fuel cell stack, ORR process is the RDS of the total stack performance. But for the traditional PEM fuel cell stack, a large impedance arc comes out in the frequency range below 1 Hz, giving equivalent contribution to the total stack impedance as ORR process. This arc is simulated as a finite diffusion process. The non-ideal EC model reflects the non-ideal characteristics of the electrodes and interfaces, and provide realistic interpretation to each impedance arc.

The impedance spectra of Nexa stack #751 measured under the current density of 100 mA cm^{-2}, 200 mA cm^{-2}, and 267 mA cm^{-2} are compared in Fig. 10, along with their fitting curves simulated from the non-ideal EC model (Fig. 3). The high frequency HOR impedance arc almost keeps stable with the increase of current density since the facile HOR does not have strong dependence on cell loads. The ORR impedance arc dominating middle frequency range significantly shrinks when the current density increases from 100 mA cm^{-2} to 200 mA cm^{-2}, but keeps almost unchanged when the current density continuously increases from 200 mA cm^{-2} to 267 mA cm^{-2}. This similar behavior to the HT-PEM fuel cell stack can also be explained as a change of RDS. When the current density is low, the charge transfer process of ORR limits the cathode

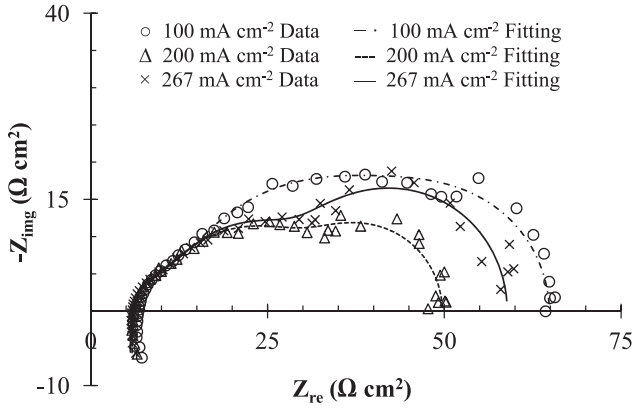

Fig. 10. Stack impedance of the traditional PEM fuel cell stack measured under *dc* current density of (○) 100 mA cm^{-2}, (Δ) 200 mA cm^{-2}, and (×) 267 mA cm^{-2}, along with their fitting curves simulated from the non-ideal EC model (Fig. 3).

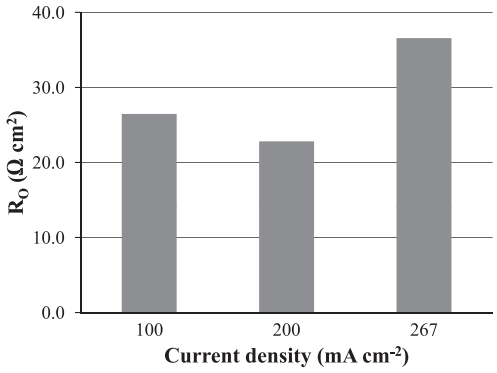

Fig. 11. The values of the equivalent diffusion resistance R_O simulated from the impedance spectra of traditional PEM fuel cell stack under changing current density.

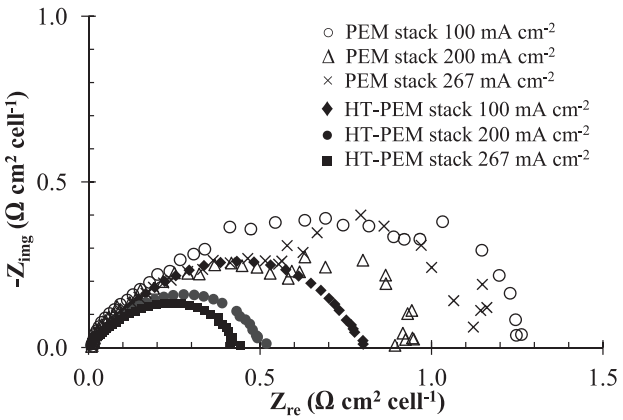

Fig. 12. Impedance comparison between the traditional PEM fuel cell stack module and the HT-PEM fuel cell stack based on a normalized impedance in the unit of Ω cm^2 $cell^{-1}$. Ohmic resistances are not included in the comparison.

performance. An increase of current density promotes ORR process and decreases its impedance. When the current density increases to a certain level, the adsorption process of ORR lags behind the charge transfer process and limits the cathode behavior.

The significant change of diffusion impedance with increasing current density shows its great dependence on the stack load. More reduced species is produced at higher current density. According to Eqs. (4) and (5), the diffusion resistance decreases when the current density changes from 100 mA cm^{-2} to 200 mA cm^{-2} (Fig. 11). However, due to the operating temperature of the traditional PEM fuel cell stack, the accumulation of liquid water inside the fuel cell at higher current densities brings challenge to the diffusion of O_2 to the cathode electrode. The diffusion of liquid water itself away from the electrode also contributes to the diffusion process. On the other side, the increased rate of O_2 consumption at higher current densities decreases the O_2 concentration in the air supplement, which also gives more impedance to the diffusion process (Eqs. (4) and (5)).

3.4. Comparison between HT-PEM and traditional PEM

To facilitate the comparison between two types of PEM fuel cell stacks, their impedance spectra are normalized to a comparable base, which is Ω cm^2 per single planar cell (Ω cm^2 $cell^{-1}$). This unit is based on the average output power density of each single cells inside the stack. Since the impedance spectra are measured from two commercial stack modules. It is difficult to separate the effects of stack control hardware from the effects of membranes and electrodes on ohmic resistances. The comparison between ohmic resistances of two modules cannot provide exact information for membrane comparison. Thus, the impedance spectra of two stacks are compared in the same Nyquist plot (Fig. 12) after subtracting ohmic resistances. The values of ohmic resistances calculated from EC simulation are used here for subtraction.

The impedance difference between two PEM fuel cell stacks at high frequency range is small, especially under low current densities. The HOR activation process on anode occurs so fast that the temperature dependence on its impedance is small. Its impedance slightly decreases when the operating temperature of the PEM fuel cell stack is elevated over 100 °C. But the difference of cathode activation impedance between two stacks is significant. The ORR activation process presents much better performance at higher operating temperature. Since the cell performance is mainly dominated by ORR process, the enhancement of its activation provides great improvement of cell performance. The finite diffusion process at low frequency range also shows large differences under different operating temperatures. The diffusion impedance arc of the HT-PEM fuel cell stack is very small and mostly overlapped by the ORR impedance arc. But the traditional PEM fuel cell stack has a large diffusion impedance arc. At low current region, the diffusion impedance decreases with increasing current density due to the faster reaction rate of ORR process. With the further increase of current density, the dependence of diffusion impedance changes. It increases with increasing current density due to the accumulation of liquid water inside the stack. This problem can be solved in the HT-PEM fuel cell systems with the single phase water environment. The higher operating temperature facilitates the water management inside the PEM fuel cells.

4. Conclusion

In this work, both a novel high temperature (HT) proton exchange membrane (PEM) fuel cell stack module operated at elevated temperatures around 160 °C and a traditional one operated at temperature between 40 °C and 65 °C were studied by impedance measurement and equivalent circuit (EC) simulation. Both PEM fuel cell stacks were manufactured at commercial level. The stack impedance measured in this work from both stacks include the impedance of ancillary components (blower, heater, sensors, embedded controller board, and any other hardware embedded in the stack modules). The impedance of ancillary components is mainly contributed to the total ohmic resistance. The stack stabilization was required before each EIS measurement to avoid significant influence of ancillary components on stack impedance. In other words, the working status of ancillary components were maintained as stable as possible during the measurement. The commercial level configuration brings more non-ideal factors to the experiments. However, more information of stack profiles during measurement are required for further analysis on impacts and deviations introduced by auxiliaries and a commercial level configuration.

One non-ideal EC model was proposed to simulate the HT-PEM fuel cell stack. The excellent goodness of fit inspired the idea to simulate the traditional PEM fuel cell stack by this non-ideal EC model. Comparing to our previous simulation with ideal EC model [17], the use of one constant phase element (CPE) Q_c and one finite diffusion element (FDE) O enhanced the simulation of the oxygen reduction reaction (ORR) process and the diffusion process at middle and low frequency range.

Based on the EC simulation and impedance interpretation, the chemical and physical processes occurring in the HT and traditional PEM fuel cell stacks were similar. The hydrogen oxidation reaction (HOR) on anode had fast kinetics no matter the operating temperature is above or below 100 °C. It contributed a small part to stack impedance. The ORR process on cathode had sluggish kinetics and dominated the total stack impedance. However, the magnitude of ORR impedance arc in the HT-PEM fuel cell stack system was much smaller than in the traditional system due to the faster kinetics at higher temperature. The elevated operating temperature of HT-PEM fuel cell stack also facilitated the O_2 diffusion process and the water management inside the stack. Thus, the diffusion impedance was decreased to a magnificent degree.

The performance of two commercial PEM fuel cell stacks were compared by EIS technique and EC simulation at a normalized impedance level. Although the application of HT-PEM fuel cells is still immature in durability, the significantly smaller polarization impedance of HT-PEM fuel cell stack gives a promising possibility to future development. This work highlights the ability of EIS and EC simulation in stack characterization and performance evaluation, and experimentally provides references for further study and diagnostics of commercial fuel cell stacks.

Acknowledgments

This work was performed under a U.S. Army contract at Auburn University (W56HZV-05-C0686) administered through TARDEC. The authors would like to thank Dr. Donald Cahela, Dr. Hongyun Yang, Mr. Dwight Cahela, and Mrs. Kimberly Dennis for their assistance and contribution to this work.

References

[1] Q.F. Li, R.H. He, J.A. Gao, J.O. Jensen, N.J. Bjerrum, J. Electrochem. Soc. 150 (2003) A1599–A1605.
[2] S.J. Peighambardoust, S. Rowshanzamir, M. Amjadi, Int. J. Hydrogen Energy 35 (2010) 9349–9384.
[3] P. Musto, F.E. Karasz, W.J. Macknight, Polymer 34 (1993) 2934–2945.
[4] S.R. Samms, S. Wasmus, R.F. Savinell, J. Electrochem. Soc. 143 (1996) 1225–1232.
[5] T.S. Chung, J. Macromol. Sci. Rev. Macromol. Chem. Phys. C37 (1997) 277–301.
[6] R.H. He, Q.F. Li, G. Xiao, N.J. Bjerrum, J. Membr. Sci. 226 (2003) 169–184.
[7] R.U. Payne, Y. Zhu, W.H. Zhu, M.S. Timper, S. Elangovan, B.J. Tatarchuk, Int. J. Electrochem. 2011 (2011) 11. Article ID 465452.
[8] J.J. Fontanella, M.C. Wintersgill, J.S. Wainright, R.F. Savinell, M. Litt, Electrochim. Acta 43 (1998) 1289–1294.
[9] R. Bouchet, E. Siebert, Solid State Ionics 118 (1999) 287–299.
[10] H. Xu, Y. Song, H.R. Kunz, J.M. Fenton, J. Electrochem. Soc. 152 (2005) A1828–A1836.
[11] V. Ramani, H.R. Kunz, J.M. Fenton, J. Power Sources 152 (2005) 182–188.
[12] N.H. Jalani, M. Ramani, K. Ohlsson, S. Buelte, G. Pacifico, R. Pollard, R. Staudt, R. Datta, J. Power Sources 160 (2006) 1096–1103.
[13] J.W. Hu, H.M. Zhang, Y.F. Zhai, G. Liu, B.L. Yi, Int. J. Hydrogen Energy 31 (2006) 1855–1862.
[14] J.W. Hu, H.M. Zhang, Y.F. Zhai, G. Liu, J. Hu, B.L. Yi, Electrochim. Acta 52 (2006) 394–401.
[15] J.W. Hu, H.M. Zhang, J. Hu, Y.F. Zhai, B.L. Yi, J. Power Sources 160 (2006) 1026–1034.
[16] W.H. Zhu, R.U. Payne, B.J. Tatarchuk, J. Power Sources 168 (2007) 211–217.
[17] W.H. Zhu, R.U. Payne, R.M. Nelms, B.J. Tatarchuk, J. Power Sources 178 (2008) 197–206.
[18] J.L. Zhang, Y.H. Tang, C.J. Song, J.J. Zhang, J. Power Sources 172 (2007) 163–171.
[19] S.J. Andreasen, J.L. Jespersen, E. Schaltz, S.K. Kaer, Fuel Cells 9 (2009) 463–473.
[20] M. Mamlouk, K. Scott, Electrochim. Acta 56 (2011) 5493–5512.
[21] J. Lobato, P. Canizares, M.A. Rodrigo, J.J. Linares, Electrochim. Acta 52 (2007) 3910–3920.
[22] M. Boaventura, A. Mendes, Int. J. Hydrogen Energy 35 (2010) 11649–11660.
[23] Q.F. Li, R.H. He, J.O. Jensen, N.J. Bjerrum, Chem. Mater. 15 (2003) 4896–4915.
[24] Q.F. Li, R.H. He, R.W. Berg, H.A. Hjuler, N.J. Bjerrum, Solid State Ionics 168 (2004) 177–185.
[25] C.Y. Chen, W.H. Lai, J. Power Sources 195 (2010) 7152–7159.
[26] R. O'Hayre, S.-W. Cha, W. Colella, F.B. Prinz, Fuel Cell Fundamentals, John Wiley & Sons, New York, Hoboken, New Jersey, 2006.
[27] Y. Oono, A. Sounai, M. Hori, J. Power Sources 189 (2009) 943–949.
[28] D.B. Sepa, M.V. Vojnovic, A. Damjanovic, Electrochim. Acta 26 (1981) 781–793.
[29] N.M. Markovic, R.R. Adzic, B.D. Cahan, E.B. Yeager, J. Electroanal. Chem. 377 (1994) 249–259.
[30] S.R. Taylor, E. Gileadi, Corrosion 51 (1995) 664–671.